Gapless Single-Spin Qubit

Maximilian Rimbach-Russ,* Valentin John, Barnaby van Straaten, and Stefano Bosco
QuTech and Kavli Institute of Nanoscience, Delft University of Technology, Delft, The Netherlands

(Received 18 December 2024; revised 6 August 2025; accepted 9 September 2025; published 3 November 2025)

All-electrical baseband control of qubits facilitates scaling up quantum processors by removing issues of crosstalk and heat generation. In semiconductor quantum dots, this is enabled by multispin qubit encodings, such as the exchange-only qubit. However, their performance is limited by unavoidable leakage states that are energetically close to the computational subspace. In this Letter, we introduce an alternative, scalable spin qubit architecture that leverages strong spin-orbit interactions of hole nanostructures for baseband qubit operations while completely eliminating leakage channels and reducing the overall gate overhead. This encoding is intrinsically robust to local variability in hole spin properties and operates with two degenerate states, removing the need for precise calibration and mitigating heat generation from fast signal sources. Finally, our architecture is fully compatible with current technology, utilizing the same initialization, readout, and multiqubit protocols of state-of-the-art spin-1/2 systems. By addressing critical scalability challenges, our design offers a robust and scalable pathway for semiconductor spin qubit technologies.

DOI: 10.1103/mvtj-zhrl

Introduction—Semiconductor quantum-dot-based spin qubits are a promising platform for large-scale and fault-tolerant quantum processors using industrial fabrication [1–6]. Among them, hole spin qubits in silicon (Si) and germanium (Ge) quantum dots are leading candidates for scaling [7–18]. Their strong spin-orbit interaction (SOI) enables ultrafast all-electric local operations [18–27] and long-distance interactions beyond the nearest neighbor [28–33]. Furthermore, SOI also provides a means to control the properties of the qubit performance *in situ*, offering sweet spots to improve the performance of the qubit [14,34–44]. In analogy to superconducting qubits, most spin qubits are controlled using microwave pulses [20,45–47], which introduce critical scaling challenges such as crosstalk and heating [48,49] posing significant barriers to the development of large-scale devices [50,51]. Progress has been made toward discrete baseband control of hole qubits through spin hopping in Ge quantum dots [18], but this approach still requires high-frequency signal generators and high-bandwidth pulses for diabatic gates, adding considerable technological constraints on electronic control.

The exchange-only (XO) qubit does not have such strict electronic requirements. The XO qubit uses multispin encoding with degenerate qubit states during idling, making phase tracking and dynamic pulse shaping obsolete and allowing electric two-axis control via interdot exchange interactions [9,52–56]. While XO qubits have shown high-fidelity single- and two-qubit gates, readout, and state initialization [57], they are heavily impacted by leakage into close-in-energy states, requiring complex pulse sequences for high-fidelity quantum gates and large overhead in fault tolerance. Furthermore, readout and initialization are also limited by additional close-in energy orbital leakage states [58].

In this Letter, we propose a novel qubit implementation by electrically tuning a hole spin qubit in the presence of strong SOI such that the qubit energy splitting, its Larmor frequency, can be tuned to zero [59]. Our resulting gapless single-spin (GS2) qubit combines the best features of XO and single spin qubits; simple and fast baseband controlled gates, no phase tracking, simple calibration, and the absence of leakage states. Remarkably, the GS2 qubit further enables a scalable architecture [see Fig. 1(a)] suppressing additional crosstalk and observer errors, multiple readout axes, and flexible high-fidelity two-qubit gates. By mitigating these key issues, our GS2 qubit encoding paves a path to scalable architectures for a full fault-tolerant quantum processors.

Architecture—Figure 1(a) shows our envisioned quantum processor architecture. Each qubit requires five gate electrodes for universal control, a central plunger gate surrounded by four control gates, thus, having a similar or smaller gate per qubit count than alternative implementations [9]. We note that the double barrier design was already demonstrated in Ref. [15] and gives rise to a

*Contact author: m.f.russ@tudelft.nl

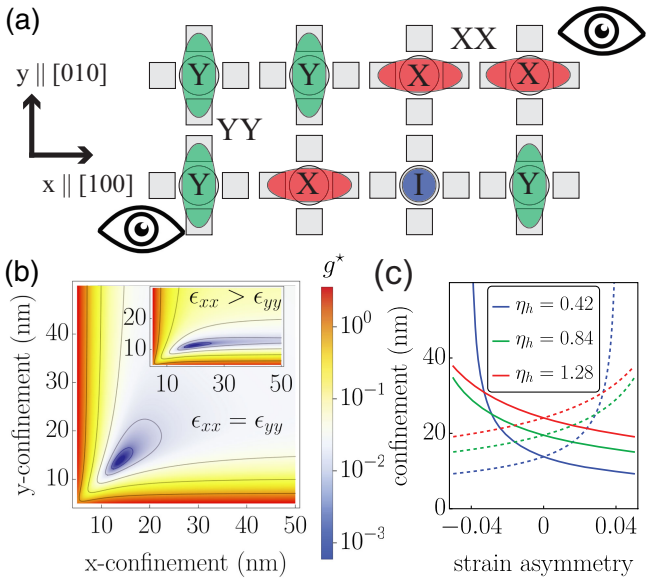

FIG. 1. (a) Proposed architecture for our novel single-spin spin-orbit qubit (GS2) qubit. Each qubit is controlled using five gate electrodes. Single-qubit gates are operated by electrically compressing and stretching the qubit. Readout, initialization, and two-qubit gates can be implemented along x and y directions. Readout and initialization uses Pauli-spin blockade and either requires a close-by charge sensor or readout resonator. During idling, qubit states are not subject to any dynamics. (b) Effective g tensor $g^\star = ||\mathcal{G}\boldsymbol{B}||/||\boldsymbol{B}||$ in the optimal optimal magnetic field direction $\boldsymbol{B}\|[110]$ (for $\boldsymbol{B}\|[1\bar{1}0]$ axes are flipped) as a function of characteristic confinement lengths of the ground state wave function in the X, Y direction, assuming biaxial strain. The GS2 qubit condition is a dot radius ≈14 nm. The inset shows GS2 conditions assuming asymmetric strain. (c) The GS2 qubit conditions for different heavy-hole light-hole coupling strengths as a function of strain asymmetry $(\epsilon_{xx} - \epsilon_{yy})/(\epsilon_{xx} + \epsilon_{yy})$.

stronger suppression of residual exchange coupling and reduced electrostatic crosstalk due to the larger spacing. At the same time, the larger separation and sparser nature of the qubit array allows easier fabrication and fan-out in contrast to dense 2D qubit arrays. By design, such a densely occupied design (with individual control) can be used to implement 2D quantum error corrections codes such as the surface code [61]. However, we note that using a sparse qubit occupation combined with hopping or shuttling interconnects [18,62] or conveying the full qubit [63,64], novel and more efficient codes may be implemented [65,66].

GS2 qubit—For our qubit encoding, we consider a single Kramers doublet of a confined particle with half-integer spin in a semiconductor quantum dot. In the presence of a magnetic field, the Hamiltonian of such a system is given by

$$H = \frac{1}{2}\mu_B \boldsymbol{\sigma} \cdot \mathcal{G}\boldsymbol{B}. \tag{1}$$

Here, $B = (B_x, B_y, B_z)^T$ is the magnetic field vector, μ_B is Bohr's magneton, and $\mathcal{G}$ is the (anisotropic) gyromagnetic matrix 3×3 [67], also called the g tensor. For our qubit design, we use two properties. First, at least two eigenvalues of the g tensor, so-called principal values, can be electrically tuned to zero. Second, the magnetic field is not collinear with one of the principal axes of the g tensor and is orthogonal to the principal axis with nonzero eigenvalue. While not exclusive, these requirements are often met in semiconductor hole qubits, e.g., hole qubits in silicon and germanium heterostructures [11,68,69].

Without loss of generality, we now consider for the remainder of the article planar germanium grown in [001] directions and prove that both requirements can be fulfilled in state-of-the-art materials. The g tensor for planar strained germanium approximately consists of three parts [70,71] $\mathcal{G} = \mathcal{G}_0 + \mathcal{G}_{\text{strain}} + \mathcal{G}_{\text{conf}}$. The first term is the bare g tensor, which for heavy-hole ground states is given by $\mathcal{G}_0 = \text{diag}(3q, -3q, 6\kappa + 27q/2)$ and is highly anisotropic $|\kappa| \gg |q|$. The second and third expressions are g-tensor corrections arising from strain and confinement.

Explicitly, considering an in-plane magnetic field, the Hamiltonian of the ground doublet is approximately

$$H = \frac{1}{2}\mu_B(B_x\mathcal{G}_{xx} + B_y\mathcal{G}_{xy})\sigma_x + \frac{1}{2}\mu_B(B_y\mathcal{G}_{yy} + B_x\mathcal{G}_{yx})\sigma_y \tag{2}$$

with the electrically tunable g-tensor components [70–74]

$$\mathcal{G}_{xx} \approx 3q - \frac{6\tilde{\kappa}b_v(\langle\epsilon_{xx}\rangle - \langle\epsilon_{yy}\rangle)}{\Delta_{\text{HL}}} - \frac{6(\lambda\langle p_x^2\rangle - \lambda'\langle p_y^2\rangle)}{m_0\Delta_{\text{HL}}}, \tag{3}$$

$$\mathcal{G}_{yy} \approx -3q - \frac{6\tilde{\kappa}b_v(\langle\epsilon_{xx}\rangle - \langle\epsilon_{yy}\rangle)}{\Delta_{\text{HL}}} + \frac{6(\lambda\langle p_y^2\rangle - \lambda'\langle p_x^2\rangle)}{m_0\Delta_{\text{HL}}}, \tag{4}$$

$$\mathcal{G}_{xy,yx} \approx \pm\frac{4\sqrt{3}\kappa d_v\epsilon_{xy}}{\Delta_{\text{HL}}} \mp \frac{12\tilde{\lambda}\langle p_x p_y\rangle}{m_0\Delta_{\text{HL}}}. \tag{5}$$

Here, the average $\langle\cdot\rangle$ is with respect to the in-plane component of the ground state wave function. The material dependent scaling parameters $\lambda = 2\eta_h\gamma_3^2 - \tilde{\kappa}\gamma_2$, $\lambda' = 2\eta_h\gamma_3\gamma_2 - \tilde{\kappa}\gamma_2$, $\tilde{\lambda} = 2\eta_h(\gamma_2\gamma_3 + \gamma_3^2) - \tilde{\kappa}\gamma_3$, and $\tilde{\kappa} = \kappa - 2\tilde{\eta}_h\gamma_3$ depend on the material dependent Luttinger parameters γ_1, γ_2, and γ_3, deformation parameters a_v, b_v, and d_v [75], and interband couplings, η_h and $\tilde{\eta}_h$ which depend on matrix elements between out-of-plane wave functions. Conveniently, η_h and $\tilde{\eta}_h$ and $\langle p_i p_j\rangle$ are electrically controllable. In principle, $\langle\epsilon_{ij}\rangle$ is also electrically tunable, although usually less predictable. In Fig. 1(b) we show the energy splitting of Hamiltonian (2) without shear strain, $\langle\epsilon_{xy}\rangle = \langle\epsilon_{xz}\rangle = \langle\epsilon_{yz}\rangle = 0$, and separable wave functions $\langle p_x p_y\rangle = \langle p_x p_z\rangle = \langle p_y p_z\rangle = 0$ with symmetric and asymmetric strain. Here, we introduced for better understanding the characteristic length of the in-plane wave

function $\langle p_i^2\rangle = \hbar^2/(2L_i^2)$ with $i = x, y$. We can clearly identify the operation regime of our GS2 qubit at characteristic confinement lengths of 10–20 nm using parameters from Ref. [70]. The zero crossings can be analytically expressed as

$$\langle p_x^2\rangle = p_{x,a}^2 = \frac{m_0}{2}\left[\frac{\Delta_{\mathrm{HL}} q}{\lambda-\lambda'} - \frac{2b_v\tilde{\kappa}(\langle\epsilon_{xx}\rangle - \langle\epsilon_{yy}\rangle)}{\lambda+\lambda'}\right], \quad (6)$$

$$\langle p_y^2\rangle = p_{y,a}^2 = \frac{m_0}{2}\left[\frac{\Delta_{\mathrm{HL}} q}{\lambda-\lambda'} + \frac{2b_v\tilde{\kappa}(\langle\epsilon_{xx}\rangle - \langle\epsilon_{yy}\rangle)}{\lambda+\lambda'}\right]. \quad (7)$$

While the required characteristic confinement lengths seem small, simulations and experimental demonstration show that they are feasible [see Supplemental Fig. GS22(b) in Ref. [18]]. In Fig. 1(c), we show the GS2 condition for varying strain asymmetry $(\epsilon_{xx}-\epsilon_{yy})/(\epsilon_{xx}+\epsilon_{yy})$ that may arise from disorder [76] and for different heavy-hole light-hole coupling strengths [77]. Conveniently, typical strain fluctuations arising from dislocations are on length scales multiple quantum dot radii [76], thus each GS2 qubit can be tuned to its own respective operation point. We also remark that the GS2 condition is predicted to be possible in other material and device structures [37,68,69].

Shear strain from metallic top gates [70] or strong confinement [78] adds terms of the form $(B_x\mathcal{G}_{zx}+B_y\mathcal{G}_{zy})\sigma_z$ to Hamiltonian (2) giving rise to errors. However, due to the interplay of confinement and strain, there still exist a confinement that fulfills our requirements (see general expressions in Ref. [71]). In practice, one wants to avoid these shear contributions, for example, through deeper quantum wells, gate designs that minimize average shear strain, or materials with a smaller differential thermal expansion coefficient.

Qubit states—The qubit states are encoded in the twofold degenerate doublet, defined as $|\uparrow,\downarrow\rangle$. Unlike conventional Loss-DiVincenzo qubits and similar to exchange-only qubits, the degeneracy ensures that our qubit has no dynamics during idling. Unlike exchange-only qubits, however, our qubit has no leakage states since only a single doublet is used and excited states are separated by more than 1 meV. Therefore, our design combines the best of both worlds. To the best of our knowledge, there is no equivalent encoding with a single particle in any quantum computing platform.

Single qubit operations—Single qubit gates are enabled by small deviations from the degeneracy condition $\langle p_x^2\rangle = p_{x,a}^2 + \langle p_x^2\rangle_\Delta$ and $\langle p_y^2\rangle = p_{y,a}^2 + \langle p_y^2\rangle_\Delta$ that lead to the standard Hamiltonian

$$H_{1q} = b_x\sigma_x + b_y\sigma_y, \quad (8)$$

with $b_{x,y} = \mp\frac{1}{2}\mu_B B_{x,y}[6/m_0\Delta_{\mathrm{HL}}](\lambda\langle p_{x,y}^2\rangle_\Delta - \lambda'\langle p_{y,x}^2\rangle_\Delta)$ and neglecting out-of-plane tilts.

Using the layout shown in Fig. 1(a), $\langle p_x^2\rangle$ and $\langle p_y^2\rangle$ can be individually and electrically controlled, giving rise to arbitrary single qubit rotations. Orthogonal rotations around the X, Y axis can be realized by pulsing $(\langle p_{x,y}^2\rangle_\Delta/\langle p_{y,x}^2\rangle_\Delta) = (\lambda/\lambda')$ [79]. Notably, a misaligned magnetic field in the x, y plane only affects the gate speed and not the rotation angle of the quantum gate. Consequently, the fastest operations are achieved if $\boldsymbol{B}\|[110]$ or $\boldsymbol{B}\|[1\bar{1}0]$. We remark that in realistic structures due to cross-capacitance coupling, orthogonal control might require an additional calibration step [80] or sufficient virtualization [81].

Potential error sources for gate operations are terms in Hamiltonian (8) proportional to σ_z and calibration errors that lead to $b_{y,x} \neq 0$ while performing X, Y operations. Fortunately, there are several techniques being able to suppress such errors. For small to medium-size σ_z terms, composite pulse sequences can be used to drastically suppress such off-resonance errors [82]. In Fig. 2(a), we show the infidelity of X operations using naive direct pules, the composite pulse short-CORPSE (sCORPSE), and the composite pulse sequence CORPSE. Conveniently, the (s) CORPSE pulse sequence for X, Y pulses only requires X, Y and $-X, -Y$ pulses, thus no additional constraint on the electronics is imposed and no additional calibration is needed. For large σ_z terms, nonadiabatic gates can be used instead [18]. We further note, that due to the degeneracy, holonomic single-qubit gates might be possible [83,84].

Analogously to almost all qubit encodings, the GS2 qubit is also affected by electric and magnetic noise. Electric noise dominantly arises from ubiquitous charge noise present in condensed matter that modifies the electrostatic confinement, changes the wave functions of the charge carrier, and affects our qubit via spin-orbit and exchange couplings. Unlike qubits with a finite frequency

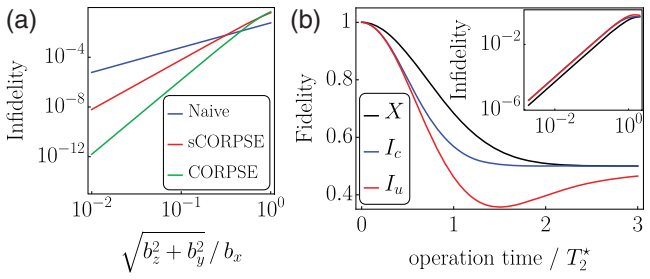

FIG. 2. (a) Single qubit gate fidelity [85] of X gates as a function of miscalibration $b_{y,z} \neq 0$ from the GS2 condition without decoherence. Three pulse techniques are shown, (blue) single pulse, (red) composite pulse sequence short-CORPSE, and (green) composite pulse sequence CORPSE. (b) Fidelity of a (black) X operation and (blue and red) idling I operation under the influence of low frequency noise coupling in via the g tensor as a function of operation time. Our simulation assumes quasi-static fluctuations in b_x and b_y, neglects transversally coupled noise for the X operation, and assumes (blue) correlated and (red) uncorrelated fluctuations between b_x and b_y.

splitting during idling, zero-frequency qubits are subject to different types of decoherence making the distinction of T_1 and T_2 times obsolete. To still provide a meaningful description, we instead report the process fidelity of gate and idling operations [85] as a function of time. By design, decoherence during an X, Y operation corresponds to the $T_2^\star$ time of conventional spin-1/2 qubits. However, note that the gate time of performing X, Y operations is given by the change in Larmor frequency instead of the Rabi frequency, which can be multiple times faster. High quality factors $f_{\mathrm{Larmor}} \times T_2^\star$ exceeding 1000 are frequently reported [10]. Using Schrödinger-Poisson simulations [86], we estimate a central gate sensitivity $\partial_{V_c}\langle p_y^2\rangle/\hbar^2 = (0.064)^2\ \mathrm{nm}^{-2}/\mathrm{V}$ giving rise to $b_x \approx 630(\mathrm{MHz/V})$ considering $B = 100$ mT, $\eta_h = 0.42$, and $\tilde{\eta}_h = 0$. Faster operations can be achieved by pulsing center and side gates simultaneously and improved gate fidelities can be gained by more sophisticated composite pulse sequence design [87].

Decoherence during idling at the degeneracy point is caused by two orthogonally coupled random fluctuations and is approximately $\sqrt{2}$ times faster with only a small dependence on their cross-correlation. In Fig. 2(b) we show the gate fidelity as a function of operation time and $T_2^\star$ for single-qubit gates X and the idling operation. Assuming a pessimistic $Q = 100$, gate infidelities above $1 - F = 10^{-4}$ for all operations are achievable. Since charge and magnetic noise is dominantly slow, dynamical decoupling protocols, such as Z echo or $XY4$ [88–90], can greatly extend coherence times. Additionally, by setting a small energy splitting Δ during idle with $2\pi\hbar/T_{\mathrm{alg}} \ll \Delta < 2\pi\hbar/T_\pi$, where T_π is the gate time of a Pauli X/Y gate and T_{alg} is the algorithm duration, the impact of ultralow frequency noise can be strongly suppressed recovering decoherence times of traditional hole qubits [91].

Magnetic noise typically originates from the hyperfine coupling to nuclear spins with nonzero spin. For planar germanium, the hyperfine tensor is highly anisotropic, thus, magnetic noise is highly suppressed for in-plane magnetic field directions. Remarkably, the GS2 operation regime coincides in some materials with the noise sweet spot [35,37]. Furthermore, the nuclear spins as a magnetic noise source can be effectively eliminated by isotopic purification [92].

Readout and initialization—The GS2 qubit can be read out using conventional Pauli-spin blockade (PSB) methods, where spin-selective charge transitions are observed. While PSB readout is generally used to read out any quantum dot spin-qubit, the unblocked spin state depends on the interplay of the Zeeman and the exchange interaction between spins in neighboring quantum dots. We distinguish three cases: (i) for a uniform magnetic field and a uniform g tensor without spin-orbit interaction, the spin singlet state $|S\rangle = (|10\rangle - |01\rangle)/\sqrt{2}$ is unblocked. We call this PSB-S and it is typically used for electron spin qubits without micromagnet, singlet-triplet, and EO qubits. (ii) For magnetic fields with a parallel gradient or a uniform magnetic field along a (common) principal axis of the g tensors without spin-orbit interaction, the $|01\rangle$ or $|10\rangle$ state is unblocked. We call this the PSB-Z and it is typically used for electron spin qubits with a micromagnet. (iii) For magnetic fields with an orthogonal gradient, a uniform magnetic field along a (common) principal axis of the g tensors, or spin-orbit interaction, the $|11\rangle$ is unblocked. We call this the PSB-T and is typically implemented for hole spin qubits.

The PSB Hamiltonian is well approximated by [93]

$$H = H_{1q}^{(A)} + H_{1q}^{(B)} + \varepsilon|S_{02}\rangle\langle S_{02}| + \sqrt{2}t_c\cos(\theta_{\mathrm{SOI}})|S\rangle\langle S_{02}| + i\sqrt{2}t_c\sin(\theta_{\mathrm{SOI}})\boldsymbol{n}\cdot|\boldsymbol{T}\rangle\langle S_{02}| + \mathrm{H.c.}, \tag{9}$$

where $H_{1q}^{(A,B)}$ is the single-qubit Hamiltonian (8) of qubit A, B, $\boldsymbol{n}$ is the normalized spin-orbit vector, θ_{SOI} the spin-flip angle, and $\boldsymbol{T}_{AB} = (T_x, T_y, T_z)^T$ is a vector consisting of the spin-1 triplet states with $|T_{x,y}\rangle = i^{1/2\mp1/2}(|00\rangle \mp |11\rangle)/\sqrt{2}$ and $|T_z\rangle = (|01\rangle + |10\rangle)/\sqrt{2}$. For planar holes, θ_{SOI} arises from cubic-in-momentum spin-orbit coupling [94] or linear-in-momentum through strain gradients [70], and can be assumed or engineered to be small [95–97]. For other platforms θ_{SOI} can be large [11].

Remarkably, our qubit can be electrically tuned into all mentioned PSB readout types [98]. For $b_x^A = b_x^B = b_y^A = b_y^B$, we find PSB-S, for $b_{x,y}^A \neq b_{x,y}^B \neq 0$ and $b_{y,x}^A = b_{y,x}^B = 0$ we find PSB-X, Y which is PSB-Z in the x, y basis, and for $b_{x,y}^A \neq b_{y,x}^B \neq 0$ we find PSB-T readout. We note, that the proposed readout methods are applicable for any hole qubits with sufficient control [99].

To avoid ambiguity, we conceive a two-step high-fidelity PSB readout and initialization protocol: (i) we elongate the wave functions such that they get closer and the tunnel coupling between the two dots is increased. For PSB-X, this leads to $b_x^{A,B} > 0$. (ii) While tilting the two dots by sweeping the detuning ε from positive to negative, we additionally compress (stretch) the first (second) wave function such that $b_y^A \approx -b_y^B$ [100]. This ensures that we open the anticrossing between the $|00\rangle$ and $|S_{02}\rangle$ states even in the presence of small θ_{SOI} to ensure PSB-T [see Fig. 3(a)]. Figure 3(b) shows the readout infidelity $1 - P_{\mathrm{read}}$ for a constant detuning pulse, where $P_{\mathrm{read}} = P_{|00\rangle\to|S_{02}\rangle} - P_{|10\rangle\to|S_{02}\rangle}$ is the readout visibility [101]. Noticeably, high-fidelity readout is achieved for the vast majority of conditions. Only for $\theta_{\mathrm{SOI}} \approx \pi/2$ and $\phi_{\mathrm{SOI}} \approx 0$ the anticrossing between $|00\rangle$ and $|S_{02}\rangle$ is closed due to the interplay between spin-orbit interaction and quantization axis rotation [25]. In germanium, PSB-T readout and initialization protocols similar to our method achieve high fidelities [99]. We further remark that faster pulses with higher fidelity can

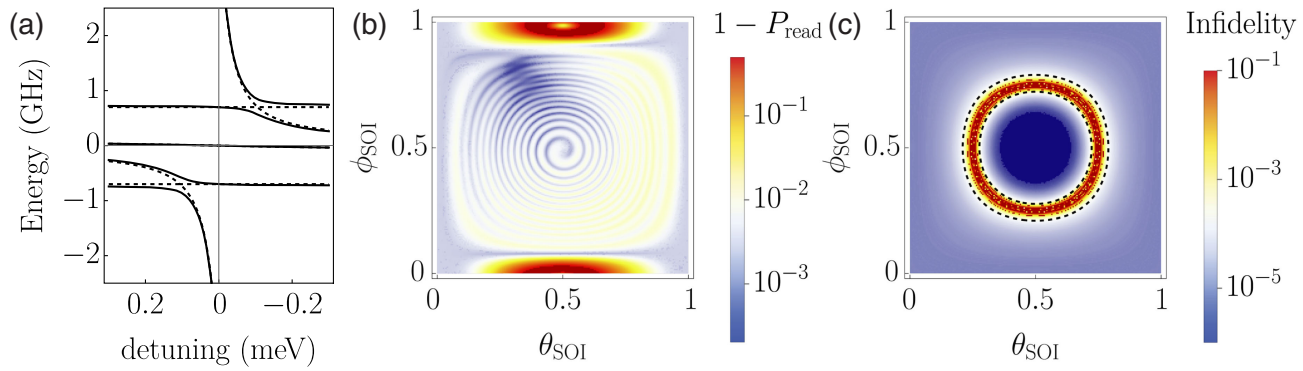

FIG. 3. (a) Energy diagram of the anticrossing used for Pauli-Spin blockade (PSB) readout as a function of detuning ε for the stabilized protocol $b_y^{(A)} = -b_y^{(B)} = 0.1$ GHz (dashed lines showing $b_y^{(A)} = b_y^{(B)} = 0$) considering $b_x^{(A)} = 0.3$ GHz, $b_x^{(B)} = 0.4$ GHz, $t_c = 3$ GHz, and $\theta_{\mathrm{SOI}} = 0$. Our protocol induces an anticrossing between $|00\rangle$ and $|S_{02}\rangle$ identical as in the presence of finite spin-orbit interaction. (b) Simulated readout infidelity of the stabilized protocol for a linear ramp from $\varepsilon(t = 0) = 0.5$ meV to $\varepsilon(t = T) = -0.5$ meV with duration $T = 52.7$ ns as a function of the spin-flip angle θ_{SOI} and SOI vector $\boldsymbol{n} = [\cos(\phi_{\mathrm{SOI}}), \sin(\phi_{\mathrm{SOI}}), 0]^T$ and using the same parameters as before. (c) Simulated average gate infidelity of an adiabatic CX two-qubit gate up to single-qubit X gates with fixed duration $T = 36$ ns using a Tukey pulse [106] as a function of θ_{SOI} and $\boldsymbol{n}$. The area between the two dashed black lines highlights the regime in which SWAP oscillations cannot be suppressed [71] and $\sqrt{\mathrm{SWAP}}$-type gates are preferred [107–109]. Simulation parameters are identical to (a) and (b). Tunneling and exchange are modeled assuming Gaussian overlaps [110]. Oscillations originate from Landau-Zener transitions.

be achieved using optimal control; especially the QUAD protocol allows for consistently high transfer fidelity [102–105]. Consequently, high-fidelity state initialization can be achieved by reversing the upper protocol.

Two qubit gates—The two qubit gates are implemented similar to traditional spin qubits using the exchange interaction originating from the wave function overlap. The interaction Hamiltonian between qubits A and B is well approximated by [17,47,111]

$$H_{2q} = H_{1q}^{(A)} + H_{1q}^{(B)} + \frac{J}{4}\boldsymbol{\sigma}^{(A)} \cdot R_{\boldsymbol{n}}(2\theta_{\mathrm{SOI}})\boldsymbol{\sigma}^{(B)}, \quad (10)$$

where J is the electrically tunable exchange coupling and $R_{\boldsymbol{n}}(2\theta_{\mathrm{SOI}})$ is the 3D rotation matrix originating from the spin-orbit interaction [111]. In our proposed architecture [Fig. 1(a)], two-qubit gates can be implemented in the X, Y direction, giving rise to a maximally entangling CNOT gate up to single-qubit rotations. Additionally, the two-qubit gate can be implemented using adiabatic or diabatic pulses [106–108]. Note that undesired evolutions during diabatic gates can be suppressed by interleaving the two-qubit interaction with single-qubit X, Y gates [7,112]. Figure 3(c) shows the average gate fidelity [85] for an adiabatic CNOT gate in the x direction with maximum qubit frequency difference $\Delta E = 200$ MHz. Noticeably, there are three regimes showing vastly different results. The outer area is the conventional adiabatic regime, where non-adiabatic SWAP oscillations are sufficiently suppressed. In the area in-between the dashed lines [71], the adiabatic condition is not fulfilled and diabatic errors dominate as the accumulated entangling phase becomes very small. In the center area, the diabatic contributions are strongly suppressed, giving rise to the highest fidelities [111]. We anticipate that the gate fidelity can be further enhanced by optimal control techniques [106,113] and combined with shuttling [114].

Conclusion—We have introduced the GS2 qubit, a qubit encoding without the need for complex control electronics, that can be controlled fully using only baseband pulses, possessing no noticeably leakage states, and allowing fast and high-fidelity two-qubit gates. Our encoding fully leverages the potential of hole qubits and spin-orbit interaction through the g tensor. Remarkably, our qubit can be implemented in state-of-the-art materials. This makes the GS2 qubit a truly promising encoding to realize a large-scale quantum processor.

Acknowledgments—We thank David DiVincenzo, Viatcheslav Dobrovitski, Edmondo Valvo, Aram Shojaei, and Menno Veldhorst (in no particular order) for fruitful discussions. We also thank all members of the Bosco, Rimbach-Russ, Veldhorst, and Vandersypen group for valuable feedback. M. R.-R. acknowledges support from NWO under Veni Grant (No. VI.Veni.212.223). This research was partly supported by the EU through the H2024 QLSI2 project and partly sponsored by the Army Research Office under Award No. W911NF-23-1-0110.

The views and conclusions contained in this document are those of the authors and should not be interpreted as representing the official policies, either expressed or implied, of the Army Research Office or the U.S. Government. The U.S. Government is authorized to

Data availability—The data that support the findings of this article are openly available [115].

[1] R. Li, N. I. D. Stuyck, S. Kubicek, J. Jussot, B. T. Chan, F. A. Mohiyaddin, A. Elsayed, M. Shehata, G. Simion, C. Godfrin, Y. Canvel, Ts. Ivanov, L. Goux, B. Govoreanu, and I. P. Radu, A flexible 300 mm integrated Si MOS platform for electron- and hole-spin qubits exploration, in *2020 IEEE International Electron Devices Meeting (IEDM)* (2020), pp. 38.3.1–38.3.4, 10.1109/IEDM13553.2020.9371956.

[2] T. Bédécarrats *et al.*, A new FDSOI spin qubit platform with 40 nm effective control pitch, in *2021 IEEE International Electron Devices Meeting (IEDM)* (2021), pp. 1–4, 10.1109/IEDM19574.2021.9720497.

[3] A. M. J. Zwerver *et al.*, Qubits made by advanced semiconductor manufacturing, Natl. Electron. Rev. **5**, 184 (2022).

[4] H. C. George *et al.*, 12-spin-qubit arrays fabricated on a 300 mm semiconductor manufacturing line, Nano Lett. **25**, 793 (2025).

[5] P. Steinacker *et al.*, A 300 mm foundry silicon spin qubit unit cell exceeding 99% fidelity in all operations, arXiv:2410.15590.

[6] T. Huckemann, P. Muster, W. Langheinrich, V. Brackmann, M. Friedrich, N. D. Komerički, L. K. Diebel, V. Stieß, D. Bougeard, Y. Yamamoto, F. Reichmann, M. H. Zoellner, C. Dahl, L. R. Schreiber, and H. Bluhm, Industrially fabricated single-electron quantum dots in Si/Si—Ge heterostructures, IEEE Electron Device Lett. **46**, 868 (2025).

[7] D. Loss and D. P. DiVincenzo, Quantum computation with quantum dots, Phys. Rev. A **57**, 120 (1998).

[8] C. Kloeffel and D. Loss, Prospects for spin-based quantum computing in quantum dots, Annu. Rev. Condens. Matter Phys. **4**, 51 (2013).

[9] G. Burkard, T. D. Ladd, A. Pan, J. M. Nichol, and J. R. Petta, Semiconductor spin qubits, Rev. Mod. Phys. **95**, 025003 (2023).

[10] P. Stano and D. Loss, Review of performance metrics of spin qubits in gated semiconducting nanostructures, Nat. Rev. Phys. **4**, 672 (2022).

[11] G. Scappucci, C. Kloeffel, F. A. Zwanenburg, D. Loss, M. Myronov, J.-J. Zhang, S. De Franceschi, G. Katsaros, and M. Veldhorst, The germanium quantum information route, Nat. Rev. Mater. **6**, 926 (2020).

[12] Y. Fang, P. Philippopoulos, D. Culcer, W. A. Coish, and S. Chesi, Recent advances in hole-spin qubits, Mater. Quantum. Technol. **3**, 012003 (2023).

[13] R. Maurand, X. Jehl, D. Kotekar-Patil, A. Corna, H. Bohuslavskyi, R. Laviéville, L. Hutin, S. Barraud, M. Vinet, M. Sanquer, and S. De Franceschi, A CMOS silicon spin qubit, Nat. Commun. **7**, 13575 (2016).

[14] N. W. Hendrickx, L. Massai, M. Mergenthaler, F. J. Schupp, S. Paredes, S. W. Bedell, G. Salis, and A. Fuhrer, Sweet-spot operation of a germanium hole spin qubit with highly anisotropic noise sensitivity, Nat. Mater. **23**, 920 (2024).

[15] F. Borsoi, N. W. Hendrickx, V. John, M. Meyer, S. Motz, F. van Riggelen, A. Sammak, S. L. de Snoo, G. Scappucci, and M. Veldhorst, Shared control of a 16 semiconductor quantum dot crossbar array, Nat. Nanotechnol. **19**, 21 (2023).

[16] V. John, F. Borsoi, Z. György, C.-A. Wang, G. Széchenyi, F. van Riggelen-Doelman, W. I. L. Lawrie, N. W. Hendrickx, A. Sammak, G. Scappucci, A. Pályi, and M. Veldhorst, Bichromatic Rabi control of semiconductor qubits, Phys. Rev. Lett. **132**, 067001 (2024).

[17] X. Zhang, E. Morozova, M. Rimbach-Russ, D. Jirovec, T.-K. Hsiao, P. C. Fariña, C.-A. Wang, S. D. Oosterhout, A. Sammak, G. Scappucci, M. Veldhorst, and L. M. K. Vandersypen, Universal control of four singlet–triplet qubits, Nat. Nanotechnol. **20**, 209 (2024).

[18] C.-A. Wang, V. John, H. Tidjani, C. X. Yu, A. S. Ivlev, C. Déprez, F. van Riggelen-Doelman, B. D. Woods, N. W. Hendrickx, W. I. L. Lawrie, L. E. A. Stehouwer, S. D. Oosterhout, A. Sammak, M. Friesen, G. Scappucci, S. L. de Snoo, M. Rimbach-Russ, F. Borsoi, and M. Veldhorst, Operating semiconductor quantum processors with hopping spins, Science **385**, 447 (2024).

[19] D. V. Bulaev and D. Loss, Electric dipole spin resonance for heavy holes in quantum dots, Phys. Rev. Lett. **98**, 097202 (2007).

[20] N. W. Hendrickx, W. I. L. Lawrie, M. Russ, F. van Riggelen, S. L. de Snoo, R. N. Schouten, A. Sammak, G. Scappucci, and M. Veldhorst, A four-qubit germanium quantum processor, Nature (London) **591**, 580 (2021).

[21] F. N. M. Froning, L. C. Camenzind, O. A. H. van der Molen, A. Li, E. P. A. M. Bakkers, D. M. Zumbühl, and F. R. Braakman, Ultrafast hole spin qubit with gate-tunable spin–orbit switch functionality, Nat. Nanotechnol. **16**, 308 (2021).

[22] L. C. Camenzind, S. Geyer, A. Fuhrer, R. J. Warburton, D. M. Zumbühl, and A. V. Kuhlmann, A hole spin qubit in a fin field-effect transistor above 4 Kelvin, Nat. Electron. **5**, 178 (2022).

[23] D. Jirovec, A. Hofmann, A. Ballabio, P. M. Mutter, G. Tavani, M. Botifoll, A. Crippa, J. Kukucka, O. Sagi, F. Martins, J. Saez-Mollejo, I. Prieto, M. Borovkov, J. Arbiol, D. Chrastina, G. Isella, and G. Katsaros, A singlet-triplet hole spin qubit in planar Ge, Nat. Mater. **20**, 1106 (2021).

[24] K. Wang, G. Xu, F. Gao, H. Liu, R.-L. Ma, X. Zhang, Z. Wang, G. Cao, T. Wang, J.-J. Zhang, D. Culcer, X. Hu, H.-W. Jiang, H.-O. Li, G.-C. Guo, and G.-P. Guo, Ultrafast coherent control of a hole spin qubit in a germanium quantum dot, Nat. Commun. **13**, 206 (2022).

[25] D. Jirovec, P. M. Mutter, A. Hofmann, A. Crippa, M. Rychetsky, D. L. Craig, J. Kukucka, F. Martins, A. Ballabio, N. Ares, D. Chrastina, G. Isella, G. Burkard, and G. Katsaros, Dynamics of hole singlet-triplet qubits with large g-factor differences, Phys. Rev. Lett. **128**, 126803 (2022).

[26] S. D. Liles, D. J. Halverson, Z. Wang, A. Shamim, R. S. Eggli, I. K. Jin, J. Hillier, K. Kumar, I. Vorreiter, M. J. Rendell, J. Y. Huang, C. C. Escott, F. E. Hudson, W. H. Lim, D. Culcer, A. S. Dzurak, and A. R. Hamilton,

A singlet-triplet hole-spin qubit in MOS silicon, Nat. Commun. **15**, 7690 (2024).
[27] H. Liu, K. Wang, F. Gao, J. Leng, Y. Liu, Y.-C. Zhou, G. Cao, T. Wang, J. Zhang, P. Huang, H.-O. Li, and G.-P. Guo, Ultrafast and electrically tunable Rabi frequency in a germanium hut wire hole spin qubit, Nano Lett. **23**, 3810 (2023).
[28] C. Kloeffel, M. Trif, P. Stano, and D. Loss, Circuit QED with hole-spin qubits in Ge/Si nanowire quantum dots, Phys. Rev. B **88**, 241405(R) (2013).
[29] P. M. Mutter and G. Burkard, Natural heavy-hole flopping mode qubit in germanium, Phys. Rev. Res. **3**, 013194 (2021).
[30] S. Bosco, P. Scarlino, J. Klinovaja, and D. Loss, Fully tunable longitudinal spin-photon interactions in Si and Ge quantum dots, Phys. Rev. Lett. **129**, 066801 (2022).
[31] V. P. Michal, J. C. Abadillo-Uriel, S. Zihlmann, R. Maurand, Y.-M. Niquet, and M. Filippone, Tunable hole spin-photon interaction based on g-matrix modulation, Phys. Rev. B **107**, L041303 (2023).
[32] C. X. Yu, S. Zihlmann, J. C. Abadillo-Uriel, V. P. Michal, N. Rambal, H. Niebojewski, T. Bedecarrats, M. Vinet, É. Dumur, M. Filippone, B. Bertrand, S. De Franceschi, Y.-M. Niquet, and R. Maurand, Strong coupling between a photon and a hole spin in silicon, Nat. Nanotechnol. **18**, 741 (2023).
[33] F. De Palma, F. Oppliger, W. Jang, S. Bosco, M. Janík, S. Calcaterra, G. Katsaros, G. Isella, D. Loss, and P. Scarlino, Strong hole-photon coupling in planar Ge for probing charge degree and strongly correlated states, Nat. Commun. **15**, 10177 (2024).
[34] P. M. Mutter and G. Burkard, All-electrical control of hole singlet-triplet spin qubits at low-leakage points, Phys. Rev. B **104**, 195421 (2021).
[35] S. Bosco, B. Hetényi, and D. Loss, Hole spin qubits in Si FinFETs with fully tunable spin-orbit coupling and sweet spots for charge noise, PRX Quantum **2**, 010348 (2021).
[36] Z. Wang, E. Marcellina, A. R. Hamilton, J. H. Cullen, S. Rogge, J. Salfi, and D. Culcer, Optimal operation points for ultrafast, highly coherent Ge hole spin-orbit qubits, npj Quantum Inf. **7**, 1 (2021).
[37] S. Bosco and D. Loss, Fully tunable hyperfine interactions of hole spin qubits in Si and Ge quantum dots, Phys. Rev. Lett. **127**, 190501 (2021).
[38] N. Piot, B. Brun, V. Schmitt, S. Zihlmann, V. P. Michal, A. Apra, J. C. Abadillo-Uriel, X. Jehl, B. Bertrand, H. Niebojewski, L. Hutin, M. Vinet, M. Urdampilleta, T. Meunier, Y.-M. Niquet, R. Maurand, and S. D. Franceschi, A single hole spin with enhanced coherence in natural silicon, Nat. Nanotechnol. **17**, 1072 (2022).
[39] S. Bosco and D. Loss, Hole spin qubits in thin curved quantum wells, Phys. Rev. Appl. **18**, 044038 (2022).
[40] C.-A. Wang, H. E. Ercan, M. F. Gyure, G. Scappucci, M. Veldhorst, and M. Rimbach-Russ, Modeling of planar germanium hole qubits in electric and magnetic fields, npj Quantum Inf. **10**, 1 (2024).
[41] A. Sen, G. Frank, B. Kolok, J. Danon, and A. Pályi, Classification and magic magnetic field directions for spin-orbit-coupled double quantum dots, Phys. Rev. B **108**, 245406 (2023).
[42] M. J. Carballido, S. Svab, R. S. Eggli, T. Patlatiuk, P. Chevalier Kwon, J. Schuff, R. M. Kaiser, L. C. Camenzind, A. Li, N. Ares, E. P. A. M. Bakkers, S. Bosco, J. C. Egues, D. Loss, and D. M. Zumbühl, Compromise-free scaling of qubit speed and coherence, Nat. Commun. **16**, 7616 (2025).
[43] L. Mauro, E. A. Rodríguez-Mena, M. Bassi, V. Schmitt, and Y.-M. Niquet, Geometry of the dephasing sweet spots of spin-orbit qubits, Phys. Rev. B **109**, 155406 (2024).
[44] S. Bosco, J. Zou, and D. Loss, High-fidelity spin qubit shuttling via large spin-orbit interactions, PRX Quantum **5**, 020353 (2024).
[45] H. Watzinger, J. Kukučka, L. Vukušić, F. Gao, T. Wang, F. Schäffler, J.-J. Zhang, and G. Katsaros, A germanium hole spin qubit, Nat. Commun. **9**, 3902 (2018).
[46] S. Bosco, S. Geyer, L. C. Camenzind, R. S. Eggli, A. Fuhrer, R. J. Warburton, D. M. Zumbühl, J. C. Egues, A. V. Kuhlmann, and D. Loss, Phase-driving hole spin qubits, Phys. Rev. Lett. **131**, 197001 (2023).
[47] J. Saez-Mollejo, D. Jirovec, Y. Schell, J. Kukucka, S. Calcaterra, D. Chrastina, G. Isella, M. Rimbach-Russ, S. Bosco, and G. Katsaros, Exchange anisotropies in microwave-driven singlet-triplet qubits, Nat. Commun. **16**, 3862 (2025).
[48] B. Undseth, X. Xue, M. Mehmandoost, M. Rimbach-Russ, P. T. Eendebak, N. Samkharadze, A. Sammak, V. V. Dobrovitski, G. Scappucci, and L. M. K. Vandersypen, Nonlinear response and crosstalk of electrically driven silicon spin qubits, Phys. Rev. Appl. **19**, 044078 (2023).
[49] B. Undseth, O. Pietx-Casas, E. Raymenants, M. Mehmandoost, M. T. Mądzik, S. G. J. Philips, S. L. de Snoo, D. J. Michalak, S. V. Amitonov, L. Tryputen, B. P. Wuetz, V. Fezzi, D. D. Esposti, A. Sammak, G. Scappucci, and L. M. K. Vandersypen, Hotter is easier: Unexpected temperature dependence of spin qubit frequencies, Phys. Rev. X **13**, 041015 (2023).
[50] M. Veldhorst, H. G. J. Eenink, C. H. Yang, and A. S. Dzurak, Silicon CMOS architecture for a spin-based quantum computer, Nat. Commun. **8**, 1766 (2017).
[51] L. M. K. Vandersypen, H. Bluhm, J. S. Clarke, A. S. Dzurak, R. Ishihara, A. Morello, D. J. Reilly, L. R. Schreiber, and M. Veldhorst, Interfacing spin qubits in quantum dots and donors—hot, dense, and coherent, npj Quantum Inf. **3**, 1 (2017).
[52] D. Bacon, J. Kempe, D. A. Lidar, and K. B. Whaley, Universal fault-tolerant quantum computation on decoherence-free subspaces, Phys. Rev. Lett. **85**, 1758 (2000).
[53] D. P. DiVincenzo, D. Bacon, J. Kempe, G. Burkard, and K. B. Whaley, Universal quantum computation with the exchange interaction, Nature (London) **408**, 339 (2000).
[54] A. Sala and J. Danon, Exchange-only singlet-only spin qubit, Phys. Rev. B **95**, 241303(R) (2017).
[55] M. Russ and G. Burkard, Three-electron spin qubits, J. Phys. Condens. Matter **29**, 393001 (2017).
[56] S. Bosco and M. Rimbach-Russ, Exchange-only spin-orbit qubits in silicon and germanium, arXiv:2410.05461.
[57] A. J. Weinstein *et al.*, Universal logic with encoded spin qubits in silicon, Nature (London) **615**, 817 (2023).

[58] D. Buterakos and S. Das Sarma, Spin-valley qubit dynamics in exchange-coupled silicon quantum dots, PRX Quantum **2**, 040358 (2021).

[59] We remark, that artificial spin-orbit interaction through micromagnets, nanomagnets, or magnetic textures can also be used instead [60].

[60] M. Aldeghi, R. Allenspach, A. Vervelaki, D. Jetter, K. Bagani, F. Braakman, M. Poggio, and G. Salis, Simulation and measurement of stray fields for the manipulation of spin qubits in one- and two-dimensional arrays, Nano Lett. **25**, 1838 (2025).

[61] D. Lidar and T. Brun, *Quantum Error Correction* (Cambridge University Press, Cambridge, England, 2013).

[62] F. van Riggelen-Doelman, C.-A. Wang, S. L. de Snoo, W. I. L. Lawrie, N. W. Hendrickx, M. Rimbach-Russ, A. Sammak, G. Scappucci, C. Déprez, and M. Veldhorst, Coherent spin qubit shuttling through germanium quantum dots, Nat. Commun. **15**, 5716 (2024).

[63] I. Seidler, T. Struck, R. Xue, N. Focke, S. Trellenkamp, H. Bluhm, and L. R. Schreiber, Conveyor-mode single-electron shuttling in Si/SiGe for a scalable quantum computing architecture, npj Quantum Inf. **8**, 1 (2022).

[64] M. De Smet, Y. Matsumoto, A.-M. J. Zwerver, L. Tryputen, S. L. de Snoo, S. V. Amitonov, S. R. Katiraee-Far, A. Sammak, N. Samkharadze, Ö. Gül, R. N. M. Wasserman, E. Greplová, M. Rimbach-Russ, G. Scappucci, and L. M. K. Vandersypen, High-fidelity single-spin shuttling in silicon, Nat. Nanotechnol. **20**, 866 (2025).

[65] S. Bravyi, A. W. Cross, J. M. Gambetta, D. Maslov, P. Rall, and T. J. Yoder, High-threshold and low-overhead fault-tolerant quantum memory, Nature (London) **627**, 778 (2024).

[66] B. Hetényi and J. R. Wootton, Tailoring quantum error correction to spin qubits, Phys. Rev. A **109**, 032433 (2024).

[67] A. Abragam and B. Bleaney, *Electron Paramagnetic Resonance of Transition Ions*, Oxford Classic Texts in the Physical Sciences (Oxford University Press, Oxford, 2012).

[68] S. Bosco, M. Benito, C. Adelsberger, and D. Loss, Squeezed hole spin qubits in Ge quantum dots with ultrafast gates at low power, Phys. Rev. B **104**, 115425 (2021).

[69] P. Del Vecchio and O. Moutanabbir, Light-hole gate-defined spin-orbit qubit, Phys. Rev. B **107**, L161406 (2023).

[70] J. C. Abadillo-Uriel, E. A. Rodríguez-Mena, B. Martinez, and Y.-M. Niquet, Hole-spin driving by strain-induced spin-orbit interactions, Phys. Rev. Lett. **131**, 097002 (2023).

[71] See Supplementary Material at http://link.aps.org/supplemental/10.1103/mvtj-zhrl for which we report complete expressions for the effective qubit Hamiltonian including locally-varying quantum dot parameters, and the complete form of the two-qubit time-evolution operator and fildeilty discussed in the main text.

[72] B. Venitucci and Y.-M. Niquet, Simple model for electrical hole spin manipulation in semiconductor quantum dots: Impact of dot material and orientation, Phys. Rev. B **99**, 115317 (2019).

[73] V. P. Michal, B. Venitucci, and Y.-M. Niquet, Longitudinal and transverse electric field manipulation of hole spin-orbit qubits in one-dimensional channels, Phys. Rev. B **103**, 045305 (2021).

[74] B. Martinez, J. C. Abadillo-Uriel, E. A. Rodríguez-Mena, and Y.-M. Niquet, Hole spin manipulation in inhomogeneous and nonseparable electric fields, Phys. Rev. B **106**, 235426 (2022).

[75] L. A. Terrazos, E. Marcellina, Z. Wang, S. N. Coppersmith, M. Friesen, A. R. Hamilton, X. Hu, B. Koiller, A. L. Saraiva, D. Culcer, and R. B. Capaz, Theory of hole-spin qubits in strained germanium quantum dots, Phys. Rev. B **103**, 125201 (2021).

[76] C. Corley-Wiciak, C. Richter, M. H. Zoellner, I. Zaitsev, C. L. Manganelli, E. Zatterin, T. U. Schülli, A. A. Corley-Wiciak, J. Katzer, F. Reichmann, W. M. Klesse, N. W. Hendrickx, A. Sammak, M. Veldhorst, G. Scappucci, M. Virgilio, and G. Capellini, Nanoscale mapping of the 3D strain tensor in a germanium quantum well hosting a functional spin qubit device, ACS Appl. Mater. Interfaces **15**, 3119 (2023).

[77] A value of $\eta_h = 0.42$ was reported in Ref. [78] assuming symmetric biaxial strain.

[78] B. Martinez, J. C. Abadillo-Uriel, E. A. Rodríguez-Mena, and Y.-M. Niquet, Hole spin manipulation in inhomogeneous and nonseparable electric fields, Phys. Rev. B **106**, 235426 (2022).

[79] Alternatively, rotations around the $\sigma_x \pm \sigma_y$-axes can be achieved by the condition $\langle p_y^2\rangle(\beta^2\lambda - \lambda') = (\beta^2\lambda' - \lambda)\langle p_x^2\rangle$ with $\beta = B_y/B_x$.

[80] F. Martins, F. K. Malinowski, P. D. Nissen, E. Barnes, S. Fallahi, G. C. Gardner, M. J. Manfra, C. M. Marcus, and F. Kuemmeth, Noise suppression using symmetric exchange gates in spin qubits, Phys. Rev. Lett. **116**, 116801 (2016).

[81] T.-K. Hsiao, C. J. van Diepen, U. Mukhopadhyay, C. Reichl, W. Wegscheider, and L. M. K. Vandersypen, Efficient orthogonal control of tunnel couplings in a quantum dot array, Phys. Rev. Appl. **13**, 054018 (2020).

[82] H. K. Cummins, G. Llewellyn, and J. A. Jones, Tackling systematic errors in quantum logic gates with composite rotations, Phys. Rev. A **67**, 042308 (2003).

[83] J. Zhang, T. H. Kyaw, S. Filipp, L.-C. Kwek, E. Sjöqvist, and D. Tong, Geometric and holonomic quantum computation, Phys. Rep. **1027**, 1 (2023).

[84] B. Kolok and A. Pályi, Protocols to measure the non-Abelian Berry phase by pumping a spin qubit through a quantum-dot loop, Phys. Rev. B **109**, 045438 (2024).

[85] The average gate fidelity is defined as $F = [1/d(d+1)](\mathrm{Tr}[(U_{\mathrm{sim}}U_{\mathrm{ideal}}^{\dagger})(U_{\mathrm{sim}}U_{\mathrm{ideal}}^{\dagger})^{\dagger}] + |\mathrm{Tr}[(U_{\mathrm{sim}}U_{\mathrm{ideal}}^{\dagger})]|^2)$, where U_{sim} and U_{ideal} are the simulated and ideal unitary matrix, respectively, and $d = 2$ for single-qubit and $d = 4$ for two-qubit operations.

[86] P. Philippopoulos, F. Beaudoin, and P. Galy, Analysis and 3D TCAD simulations of single-qubit control in an industrially-compatible FD-SOI device, Solid State Electron. **215**, 108883 (2024).

[87] T. Ichikawa, M. Bando, Y. Kondo, and M. Nakahara, Designing robust unitary gates: Application to concatenated composite pulses, Phys. Rev. A **84**, 062311 (2011).

[88] T. Gullion, D. B. Baker, and M. S. Conradi, New, compensated Carr-Purcell sequences, J. Magn. Reson. (1969) **89**, 479 (1990).

[89] Z.-H. Wang, W. Zhang, A. M. Tyryshkin, S. A. Lyon, J. W. Ager, E. E. Haller, and V. V. Dobrovitski, Effect of pulse

error accumulation on dynamical decoupling of the electron spins of phosphorus donors in silicon, Phys. Rev. B **85**, 085206 (2012).

[90] Z.-H. Wang, G. de Lange, D. Ristè, R. Hanson, and V. V. Dobrovitski, Comparison of dynamical decoupling protocols for a nitrogen-vacancy center in diamond, Phys. Rev. B **85**, 155204 (2012).

[91] We note that in this case dynamical decoupling is required to suppress the phase accumulations necessary for operating with a global clock.

[92] O. Moutanabbir, S. Assali, A. Attiaoui, G. Daligou, P. Daoust, P. D. Vecchio, S. Koelling, L. Luo, and N. Rotaru, Nuclear spin-depleted, isotopically enriched ^{70}Ge/^{28}Si^{70}Ge quantum wells, Adv. Mater. **36**, 2305703 (2024).

[93] J. Danon and Yu. V. Nazarov, Pauli spin blockade in the presence of strong spin-orbit coupling, Phys. Rev. B **80**, 041301(R) (2009).

[94] E. Marcellina, A. R. Hamilton, R. Winkler, and D. Culcer, Spin-orbit interactions in inversion-asymmetric two-dimensional hole systems: A variational analysis, Phys. Rev. B **95**, 075305 (2017).

[95] M. Lodari, O. Kong, M. Rendell, A. Tosato, A. Sammak, M. Veldhorst, A. R. Hamilton, and G. Scappucci, Lightly strained germanium quantum wells with hole mobility exceeding one million, Appl. Phys. Lett. **120**, 122104 (2022).

[96] L. E. A. Stehouwer, A. Tosato, D. Degli Esposti, D. Costa, M. Veldhorst, A. Sammak, and G. Scappucci, Germanium wafers for strained quantum wells with low disorder, Appl. Phys. Lett. **123**, 092101 (2023).

[97] C. C. D. Frink, B. D. Woods, M. P. Losert, E. R. MacQuarrie, M. A. Eriksson, and M. Friesen, Reducing strain fluctuations in quantum dot devices by gate-layer stacking, arXiv:2312.09235.

[98] For the case $\theta_{\mathrm{SOI}} \neq m\pi$ with integer m the g tensor must be additionally tuned to compensate the additional rotation.

[99] E. G. Kelly, L. Massai, B. Hetényi, M. Pita-Vidal, A. Orekhov, C. Carlsson, I. Seidler, K. Tsoukalas, L. Sommer, M. Aldeghi, S. W. Bedell, S. Paredes, F. J. Schupp, M. Mergenthaler, A. Fuhrer, G. Salis, and P. Harvey-Collard, Identifying and mitigating errors in hole spin qubit readout, arXiv:2504.06898.

[100] In practice, maintaining the condition $b_y^A = b_y^B = 0$ during the readout process might be challenging. The only strict requirement for our protocol is to first turn on one axis and then maintain adiabaticity while turning on the other parameter.

[101] A. E. Seedhouse, T. Tanttu, R. C. C. Leon, R. Zhao, K. Y. Tan, B. Hensen, F. E. Hudson, K. M. Itoh, J. Yoneda, C. H. Yang, A. Morello, A. Laucht, S. N. Coppersmith, A. Saraiva, and A. S. Dzurak, Pauli blockade in silicon quantum dots with spin-orbit control, PRX Quantum **2**, 010303 (2021).

[102] D. Fernández-Fernández, Y. Ban, and G. Platero, Quantum control of hole spin qubits in double quantum dots, Phys. Rev. Appl. **18**, 054090 (2022).

[103] F. Fehse, M. David, M. Pioro-Ladrière, and W. A. Coish, Generalized fast quasiadiabatic population transfer for improved qubit readout, shuttling, and noise mitigation, Phys. Rev. B **107**, 245303 (2023).

[104] C. V. Meinersen, S. Bosco, and M. Rimbach-Russ, Quantum geometric protocols for fast high-fidelity adiabatic state transfer, arXiv:2409.03084.

[105] C. V. Meinersen, D. Fernandez-Fernandez, G. Platero, and M. Rimbach-Russ, Unifying adiabatic state-transfer protocols with (α, β)-hypergeometries, arXiv:2504.08031.

[106] M. Rimbach-Russ, S. G. J. Philips, X. Xue, and L. M. K. Vandersypen, Simple framework for systematic high-fidelity gate operations, Quantum Sci. Technol. **8**, 045025 (2023).

[107] G. Burkard, D. Loss, D. P. DiVincenzo, and J. A. Smolin, Physical optimization of quantum error correction circuits, Phys. Rev. B **60**, 11404 (1999).

[108] T. Meunier, V. E. Calado, and L. M. K. Vandersypen, Efficient controlled-phase gate for single-spin qubits in quantum dots, Phys. Rev. B **83**, 121403(R) (2011).

[109] L. Petit, M. Russ, G. H. G. J. Eenink, W. I. L. Lawrie, J. S. Clarke, L. M. K. Vandersypen, and M. Veldhorst, Design and integration of single-qubit rotations and two-qubit gates in silicon above one Kelvin, Commun. Mater. **3**, 1 (2022).

[110] G. Burkard, D. Loss, and D. P. DiVincenzo, Coupled quantum dots as quantum gates, Phys. Rev. B **59**, 2070 (1999).

[111] S. Geyer, B. Hetényi, S. Bosco, L. C. Camenzind, R. S. Eggli, A. Fuhrer, D. Loss, R. J. Warburton, D. M. Zumbühl, and A. V. Kuhlmann, Anisotropic exchange interaction of two hole-spin qubits, Nat. Phys. **20**, 1152 (2024).

[112] M. Russ, D. M. Zajac, A. J. Sigillito, F. Borjans, J. M. Taylor, J. R. Petta, and G. Burkard, High-fidelity quantum gates in Si/SiGe double quantum dots, Phys. Rev. B **97**, 085421 (2018).

[113] İ. Polat, R. W. J. Overwater, M. Rimbach-Russ, and F. Sebastiano, Pulse shaping for ultra-fast adiabatic quantum gates, arXiv:2508.02902.

[114] Y. Matsumoto, M. D. Smet, L. Tryputen, S. L. de Snoo, S. V. Amitonov, A. Sammak, M. Rimbach-Russ, G. Scappucci, and L. M. K. Vandersypen, Two-qubit logic and teleportation with mobile spin qubits in silicon, arXiv:2503.15434.

[115] M. Rimbach-Russ, V. John, B. van Straaten, and S. Bosco, Zenodo repository, 2025, 10.5281/zenodo.17137077.